Evidence and Characterization of a New Decamolybdocobaltate Cobalt Salt: An Efficient Precursor for Hydrotreatment Catalyst Preparation

Catherine Martin,[†] Carole Lamonier,*[,†] Michel Fournier,[†] Olivier Mentré,[‡] Virginie Harlé,[‡] Denis Guillaume,[§] and Edmond Payen[†]

Laboratoire de Catalyse de Lille, UMR CNRS No. 8010, Université des Sciences et Technologies de Lille, Bâtiment C3, 59650 Villeneuve d'Ascq, France, Laboratoire de cristallochimie et physicochimie du solide de Lille, UMR CNRS No. 8012, ENSCL, BP 108, 59650 Villeneuve d'Ascq, France, and Institut Français du Pétrole, Direction Catalyse et Séparation, Institut Français du Pétrole—Lyon, BP3, 69390 Vernaison, France

Received February 17, 2005. Revised Manuscript Received June 22, 2005

Heteropolyanions (HPAs) based on molybdenum and cobalt could be used as an alternative to the conventional ammonium heptamolybdate and cobalt nitrate precursors for the preparation of Co−Mo/Al_2O_3 hydrotreating catalysts. With this objective in mind, a cobalt salt of decamolybdocobaltate anion has been synthesized. This salt allows us to prepare catalyst with a Co/Mo atomic ratio of 0.5 corresponding to the optimum value encountered with classical catalyst preparation. The crystal structure refinement has been performed and reveals the formation of a new heteropolyoxomolybdate related to the well-known Anderson structure. Its structural, spectroscopic, and thermal properties have been investigated by physical techniques such as thermogravimetric analysis mass spectroscopy, X-ray diffraction, X-ray absorption spectroscopy, and vibrational spectroscopy. With the use of this new HPA precursor, initial catalytic results show a significant improvement of hydrodesulfurization catalytic performance.

Introduction

Heteropolyanions (HPAs) are early transition-metal oxygen anion clusters that exhibit catalytic properties depending on their composition, molecular size, and structure. Molybdenum Keggin-type HPAs are particularly used in numerous oxidation or isomerization reactions.[1,2] In the field of hydrodesulfurization (HDS), the HPA applications are less conventional, but it has been shown that preparations based on the use of heteropolyoxomolybdates as starting materials could be an interesting alternative route leading to the improvement of the catalytic performances.[3,4] In this case the HPAs replace the usual ammonium heptamolybdate (AHM) and cobalt nitrate precursors. Thus, we developed the preparation of cobalt salts of Keggin phosphomolybdate for the preparation of CoMo-based catalysts,[5,6] but the Co/Mo atomic ratio was lower than the optimum ratio Co/Mo = 0.5 defined for classical preparations. Recent results now suggest that, during the classical catalyst preparation, with the AHM as the starting material, well-dispersed 6-molybdoaluminate Anderson entities are formed, and, recently, Cabello et al. proposed the use of the 6-molybdocobaltate ammonium salt, for example, the $(NH_4)_3CoMo_6O_{24}H_6$, a HPA with the Anderson structure.[7] In this new starting material the Co and the Mo atoms are inserted in the same molecular entity, which would provide a catalytic improvement according to the van Veen principle.[8] But the Co/Mo ratio is too low, and we recently proposed the use of cobalt salt of this Anderson-type HPA, $(Co)_{3/2}CoMo_6O_{24}H_6$.[9] The use of the $(NH_4)_6(Co_2Mo_{10}O_{38}H_4)\cdot 7H_2O$ salt was also proposed by Cabello et al. The cobalt salt of this decamolybdocobaltate HPA, $Co_2Mo_{10}O_{38}H_4^{6-}$, appears as a good starting material as it would allow us to reach the Co/Mo optimum ratio. We, therefore, tackled the preparation of this cobalt salt. Even if interest in compounds based on Anderson structure is maturing in the literature, only a few works deal with the dimeric HPA $Co_2Mo_{10}O_{38}H_4^{6-}$, this anion being always associated with the ammonium countercations. Friedheim and Keller[10] first showed that a secondary product with the ratio Co/Mo = 0.5 is formed during the synthesis of the ammonium salt of $CoMo_6O_{24}H_6^{4-}$ from a solution containing cobalt(II), AHM, and an oxidizing agent. Tsigdinos[11] established by a combination of results obtained from elemental

* To whom correspondence should be addressed. E-mail: carole.lamonier@univ-lille1.fr.
[†] Université des Sciences et Technologies de Lille.
[‡] ENSCL.
[§] Institut Français du Pétrole—Lyon.

(1) Liu, H. C.; Iglesia, E. *J. Phys. Chem. B* **2003**, *107* (39), 10840−10847.
(2) Okuhara, T.; Mizuno, N.; Misono, M. *Appl. Catal.* **2001**, *222*, 63−77.
(3) Spozhakina, A.; Damyanova, S.; Sharkova, V.; Shopov, D. *Proc. VIth Int. Symp. Heterogeneous Catalysis* **1987**, Part 1, 503−508.
(4) Cheng, W. C.; Luthra, N. P. *J. Catal.* **1988**, *109*, 163−169.
(5) Griboval, A.; Blanchard, P.; Payen, E.; Fournier, M.; Dubois, J. L. *Stud. Surf. Sci. Catal.* **1997**, *106*, 181−194.
(6) Griboval, A.; Blanchard, P.; Gengembre, L.; Payen, E.; Fournier, M.; Dubois, J. L.; Bernard, J. L. *J. Catal.* **1999**, *188* (1), 102−110.
(7) Cabello, C. I.; Botto, I. L.; Thomas, H. J. *Appl. Catal., A* **2000**, *197*, 79−86.
(8) van Veen, J. A. R.; Hendriks, P. A. J. M.; Andrea, R. R.; Romers, E. J. G. M.; Wilson, A. E. *J. Phys. Chem.* **1990**, *94*, 5282−5285.
(9) Martin, C.; Lamonier, C.; Michel, F.; Mentré, O.; Harlé, V.; Guillaume, D.; Payen, E. *Inorg. Chem.* **2004**, *43* (15), 4636−4641.
(10) Friedheim, C.; Keller, F. *Ber. Dtsch. Chem. Ges.* **1906**, *39*, 4301.
(11) Tsigdinos, G., Ph.D. Thesis. Boston University, Boston, MA, 1961.

10.1021/cm0503634 CCC: $30.25
Published on Web 07/16/2005

analysis, potentiometric titrations, dehydratation experiments, magnetic measurements, and absorption spectra that, in solution and in the presence of activated charcoal or Raney nickel, the Anderson species are converted entirely into dimeric ones. This ammonium salt structure has been completed by Evans and Showell leading to the proper formula $(NH_4)_6(Co_2Mo_{10}O_{38}H_4)\cdot 7H_2O$.[12] However, these authors specify that from the initial solution two crystallographic forms of ammonium salts are obtained simultaneously, namely, form A and form B, and only the latter form was crystallographically investigated. More recently, Cheng and Pereira mentioned that the rise of pH that occurs during the deposition of the 6-molybdocobaltate ammonium entity on an alumina support induces its conversion into the dimeric 5-molybdocobaltate salt.[13] Nolan et al.[14] reported a study of the mechanism of formation of the dimeric anion by peroxomonosulfate oxidation of Co^{2+} in the presence of molybdate. Finally, only two references deal with the application of this HPA in catalysis: Cabello et al. prepared the A form of the ammonium decamolybcobaltate for its use as starting material for the preparation of HDS oxidic precursor[15] and, very recently, Bravo-Suarez et al. expected that $[Co_2Mo_{10}O_{38}H_4^{6-}]$ intercalated layered double hydroxides could be used as shape-selective catalysts.[16] Both claimed that these HPAs can be used in catalysis; however, for the HDS the Co/Mo ratio is too low.

In this work, we, therefore, tackled the preparation of the $Co_2Mo_{10}O_{38}H_4^{6-}$ cobalt salt, this compound being obtained through the anionic exchange of the ammonium cation of the ammonium $Co_2Mo_{10}O_{38}H_4^{6-}$ salt. Structural investigations of the bulk salts by X-ray diffraction (XRD) analysis and X-ray absorption spectroscopy (XAS) spectroscopy have been performed confirming the preparation of the B form according to Evans' nomenclature.[12] A complete set of data have also been obtained by various spectroscopic characterizations (IR, Raman, and UV−visible) and thermogravimetric analysis mass spectroscopy (TGA-MS) analysis, which would allow us to characterize the solid after its deposition on the alumina support. Moreover, the first catalytic results in thiophene HDS obtained with catalysts prepared with this new heteropolycompound are reported.

Experimental Section

Synthesis. *$Co_2Mo_{10}Am$ Preparation*. The ammonium salt of the dimeric Anderson-based compounds, $(NH_4)_6[Co_2Mo_{10}O_{38}H_4]$ (hereafter named $Co_2Mo_{10}Am$) is obtained in very small yield in the preparation of the 6-molybdocobaltate Anderson compound, this latter being obtained by adding hydrogen peroxide in a mixed aqueous solution of AHM and cobalt nitrate. The presence of active charcoal or Raney nickel induces the quantitative formation of $Co_2Mo_{10}Am$ in solution.[11] The synthesis of $Co_2Mo_{10}Am$ was then accomplished by dissolving 75 g (0.061 mol) of $(NH_4)_6Mo_7O_{24}\cdot 4H_2O$ in 225 mL of water upon stirring in which was added dropwise an aqueous $Co(CH_3COO)_2\cdot 4H_2O$ pink solution [15.5 g (0.062 mol) dissolved in 400 mL of water]. A total of 15 g of active charcoal and 100 mL of peroxide solution (18%) were added, which induces a color change to black. After boiling the black solution for 1 h, the active charcoal is separated by filtration.

Table 1. Description and Nomenclature of the Co_2Mo_{10} Compounds

salt formula	nomenclature	Co/Mo (theorical)	Co/Mo (chemical analysis)	N/Mo (chemical analysis)
$(NH_4)_6Co_2Mo_{10}O_{38}H_4$	$Co_2Mo_{10}Am$	0.20	0.18	0.59
$Co_3Co_2Mo_{10}O_{38}H_4$	$Co_2Mo_{10}Co$	0. 50	0.49	0.01

$Co_2Mo_{10}Am$ Crystallization. Slow evaporation of the solvent at room temperature led to dark-green crystals of $Co_2Mo_{10}Am$. The recrystallization leads to their purification. The single-crystal XRD analysis indicates the preparation of $(NH_4)_6[Co_2Mo_{10}O_{38}H_4]\cdot 7H_2O$.

Cobalt Exchange. The cobalt salt was obtained by cationic exchanges in aqueous solution according to a method described in a previous paper,[9] in which is also described the preparation of the cobalt phosphomolybdate salt ($Co_{3/2}PMo_{12}O_{40}$), the Co precursor for the ionic exchange. This latter one was prepared as follows: after neutralization of a pure heteropolyacid $H_3PMo_{12}O_{40}$ solution with a solution of barium hydroxide to prepare $Ba_{3/2}PMo_{12}O_{40}$, the $Co_{3/2}PMo_{12}O_{40}$ is obtained by adding cobalt sulfate to this solution.

$$3/2\ Ba^{2+},\ PMo_{12}O_{40}^{3-} + 3/2(Co^{2+},\ SO_4^{2-}) \rightarrow (3/2Co^{2+},\ PMo_{12}O_{40}^{3-}) + 3/2\ BaSO_4\downarrow$$

The solution used for the cationic exchange is obtained by filtration, the exchange then proceeding according to the reaction:

$$6(NH_4)^+, Co_2Mo_{10}O_{38}H_4^{6-} + 2[3/2Co^{2+}, PMo_{12}O_{40}^{3-}] \rightarrow 3Co^{2+}, Co_2Mo_{10}O_{38}H_4^{6-} + 2\ (NH_4)_3PMo_{12}O_{40}\downarrow$$

The reactants are introduced into stoichiometric quantities and stirred vigorously at 50 °C for 2 h. The very low solubility of the phosphomolybdic ammonium salt induces its quantitative precipitation, and it is separated from the solution by filtration; the remaining solution containing only Co^{2+} and $Co_2Mo_{10}O_{38}H_4^{6-}$ ions is then put at 20 °C to have germination and growth of $Co_3Co_2Mo_{10}O_{38}H_4$ crystals.

TGA-MS Analysis. The TGA/differential scanning calorimetry experiments have been carried out on a 2960 SDT thermoanalyzer from TA Instruments. The TGA measurements have been carried out in a He flow of 100 mL/min, with a heating rate of 3 °C/min. The temperature was raised to 550 °C. For some experiments, the thermoanalyzer was coupled to a mass quadripolar spectrometer, from BALZERS (Omnistar model).

Single-Crystal and Powder XRD. For both $Co_2Mo_{10}Co$ and $Co_2Mo_{10}Am$, a single crystal was selected and mounted on a glass fiber. The data collection was performed using a Bruker SmartCCD-1K diffractometer. The two-dimensional detector was set at 45 mm from the crystal. One full reciprocal sphere was collected at room temperature (3 × 600 frames at $\varphi = 0$, 120, 240°, 0.3° ω scan/frame, 20 s acquisition time). Data collection, crystal characteristics, and refinement results are presented in Table 2. Intensities have been integrated from the collected frames and corrected for background, Lorentz, and polarization effects using SAINT[17] and for absorption using faces indexation and the XPREP software.[18] Data were then recorrected from the air and detector area absorption

(12) Evans, H. T. J.; Showell, S. J. *J. Am. Chem. Soc.* **1969**, *91* (24), 6881−6882.
(13) Cheng, W. C.; Pereira, C. J. *Appl. Catal.* **1987**, *33*, 331−341.
(14) Nolan, A. L.; Burns, R. C.; Lawrance, G. A. *J. Chem. Soc., Dalton Trans.* **1996**, 2629−2636.
(15) Cabello, C. I.; Cabrerizo, F.; Alvarez, A.; Thomas, H. J. *J. Mol. Catal.* **2002**, *186* (1−2), 89−100.
(16) Bravo-Suarez, J. J.; Paez-Mozo, E. A.; Oyama, S. T. *Chem. Mater.* **2004**, *16*, 1214.

Table 2. Crystal Data, Data Collection, and Structure Refinement Parameters for $(NH_4)_6[Co_2^{III}Mo_{10}H_4O_{38}]\cdot H_2O$ (compound I) and $[Co_2^{III}Mo_{10}H_4O_{38}\{Co^{II}(H_2O)_5\}_2]\cdot(Co^{II}(H_2O)_6)_1\cdot 9H_2O$ (compound II)

	compound **I**	compound **II**
crystal symmetry	monoclinic	
space group	*Pn*	*Cc*
unit cell (Å)	$a = 12.581(1)$	$a = 15.700(5)$
	$b = 12.720(1)$	$b = 13.050(5)$
	$c = 13.913(1)$	$c = 26.980(5)$
	$\beta = 108.74(1)°$	$\beta = 105.71(1)°$
volume (Å^3)	2108.38	5321.23
Z	2	4
calculated density (g/cm^3), μ (cm^{-1}) for Mo Kα	3.03, 37.32	2.85, 39.28
radiation Mo Kα (Å)	0.710 73	
recorded angular range θ (deg)	0.89−31.51	1.57−31.46
number of independent reflections [$I > \sigma(I)$]	11 522	14 270
number of independent reflections [$I > 2\sigma(I)$]	9882	13 695
transmission factor range	0.198/0.411	0.183/0.524
R merging factor (%)	3.80	3.18
number of refined parameters	588[a]	571[a]
R1	4.44	3.91
wR2	11.61[b]	9.42[b]
w[c]	$A = 0.133$, $B = 0.0$	$A = 0.0515$, $B = 0.0$
isotropic secondary extinction	none	0.000 009(15)
max/min $\Delta\rho$ (e/Å^3)	2.48, −1.46	1.48, −0.79
GOF	0.673	1.051

[a] $R1(F)[I > 2\sigma(I)] = \sum||F_o| - |F_c||/\sum|F_o|$ (%). [b] $wR2(F^2)[I > 2\sigma(I)] = [\sum w(F_o^2 - F_c^2)^2/\sum w(F_o^2)]^{1/2}$. [c] (%), $w = 1/[\sigma^2(F_o^2) + (AP)^2 + (BP)]$ with $P = [\max(F_o^2, 0) + 2F_c^2]/3$.

with a null μr value using the program SADABS.[19] Lattice parameters have been refined from the complete data set. The metal positions were determined using SIR-97.[20] The crystal structure was then refined using SHELXTL.[21] The coordination oxygen atoms and interstitial groups were located on the subsequent Fourier difference synthesis calculations. For the ammonium salt, it has not been possible to distinguish between the interstitial NH_4^+ groups and water molecules. In the last cycles of the refinement, anisotropic thermal parameters have been considered for all atoms and the introduction of an optimized weighting scheme yielded the final R1 = 4.44%, wR2 = 11.61%. For the cobalt salt, considering the high thermal vibration of the nine H_2O (labeled OH_{21-9}), their thermal parameters have been restrained equally and isotropically considered. Secondary extinction has been refined, and the introduction of an optimized weighting scheme yielded R1 = 3.91% and wR2 = 9.42%.

Powder XRD patterns were also recorded using a Siemens D5000 diffractometer with Cu Kα radiation. Apart from the Kα$_2$ contribution eliminated by computer post-processing, the patterns obtained were not subjected to further treatments.

XAS. Mo and Co K-edge EXAFS (extended X-ray absorption fine structure) measurements were carried out in the Laboratoire pour l'Utilisation du Rayonnement Electromagnétique (LURE-Orsay), at the EXAFS D42 and D44 beamlines, using synchrotron radiation from the DCI storage ring, running at 1.85 GeV with an average current of 250 mA. At the Mo K edge, the EXAFS data were taken in the transmission mode through a double-crystal monochromator Ge(400) using two ion chambers as detectors. The analysis time for an XAS spectrum (19 900−20 900 eV) was about 15 min, and three spectra were averaged for each sample. The X-ray absorption near-edge structure (XANES) data were recorded through the same monochromator, using three ion chambers as detectors, a molybdenum foil being placed after the sample to calibrate the energy position. The analysis time for a XANES spectrum (19 900−20 200 eV) was about 10 min, and two spectra have been averaged for each sample. At the Co K edge, the EXAFS data were taken in the transmission mode through a channel-cut monochromator Si-(111) using two ion chambers as detectors. The analysis time for an XAS spectrum (7600−8600 eV) was about 30 min, and five spectra are averaged for each sample. The XANES data were taken in the transmission mode through a double crystal monochromator Si(311) using three ion chambers as detectors, a cobalt foil being placed after the sample to calibrate the energy position. The analysis time for a XANES spectrum (7680−7830 eV) was about 15 min, and two spectra were recorded for each sample.

The Mo and Co K-edges EXAFS regions of the spectra were extracted and analyzed using A. Michalowicz's software packages EXAFS 98 ppc and Round Midnight.[22] The EXAFS spectrum was first transformed from k space (k^3, Kaiser window 3.7−13.3 Å^{-1} for the Mo K-edge and 2.2−14.9 Å^{-1} for the Co K-edge) to R space to obtain the radial distribution function (RDF). The EXAFS spectrum for one or several coordination shells was isolated by inverse Fourier transform of the RDF over the appropriate region and fitted using the single scattering EXAFS equation with amplitude and phase functions calculated by FEFF[23−26] from the data generated by XRD single-crystal analysis (distances between each concerned atom).

UV−Visible Spectroscopy. The diffuse reflectance spectroscopy (DRS) spectra were recorded with a Perkin-Elmer type spectrophotometer in the diffuse reflectance mode with an integrating sphere. The range covered was 170−800 nm using $BaSO_4$ as the reference.

Vibrational Spectroscopies. The IR spectra were recorded using a Fourier transform spectrophotometer (Nicolet protégé 460). The samples were analyzed using the KBr pellet technique with 1 wt % sample in KBr. The Raman spectra of the samples, maintained at room temperature, were recorded using a Raman microprobe (Infinity from Jobin-Yvon), equipped with a photodiode array detector. The exciting light source was the 532 nm line of a Nd:YAG laser, and the wavenumber accuracy was 2 cm^{-1}.

Catalytic Activity. Catalytic activities for thiophene HDS were measured at atmospheric pressure in a flow-bed reactor packed with 200 mg of catalyst. The catalysts were prepared by incipient wetness impregnation of a γ-Al_2O_3 with solution containing the appropriate amounts of molybdenum, the $Co_3Co_2Mo_{10}O_{38}H_4$ being dissolved in water. For comparison purposes, reference catalysts with the same metal loading have been prepared by the standard impregnation method using a solution containing AHM and cobalt nitrate. The impregnated alumina extrudates were dried at 353 K overnight and then calcined at 673 K under O_2 for 4 h. The solids were then sulfided in the catalytic reactor at 673 K for 2 h under a flow (100

(17) *SAINT*; area detector integration software; Siemens Industrial Automation I: Madison, WI, 1995.
(18) Sheldrick, G. M. *XPREP*; University of Gottingen: Gottingen, Germany, 1997.
(19) *SADABS*; area-detector absorption correction; Siemens Industrial Automation I: Madison, WI, 1996.
(20) Altomare, A.; Bural, M. C.; Camalli, M.; Cascarano, G. L.; Giacovazzo, C.; Guagliardi, A.; Moliterni, A. G. G.; Polidori, G.; Spagna, R. *J. Appl. Crystallogr.* **1999**, *32*, 115−119.
(21) Sheldrick, G. M. *SHELTXL 97*; program for the refinement of crystal structures; University of Gottingen: Gottingen, Germany, 1997.
(22) Michalowicz, A. *J. Phys. IV* **1997**, *7* (C2).
(23) Ankoudinov, A. L. Ph.D. Thesis; University of Washington: Seattle, WA, 1996.
(24) Rehr, J. J.; Mustre de Leon, J.; Zabinsky, S. I.; Albers, R. C. *J. Am. Chem. Soc.* **1991**, *113*, 5135.
(25) Rehr, J. J.; Zabinsky, S. I.; Albers, R. C. *Phys. Rev. Lett.* **1992**, *69*, 3397.
(26) Zabinsky, S. I.; Rehr, J. J.; Ankudinov, A.; Albers, R. C.; Eller, M. J. *Phys. Rev. B* **1995**, *52*, 2995.

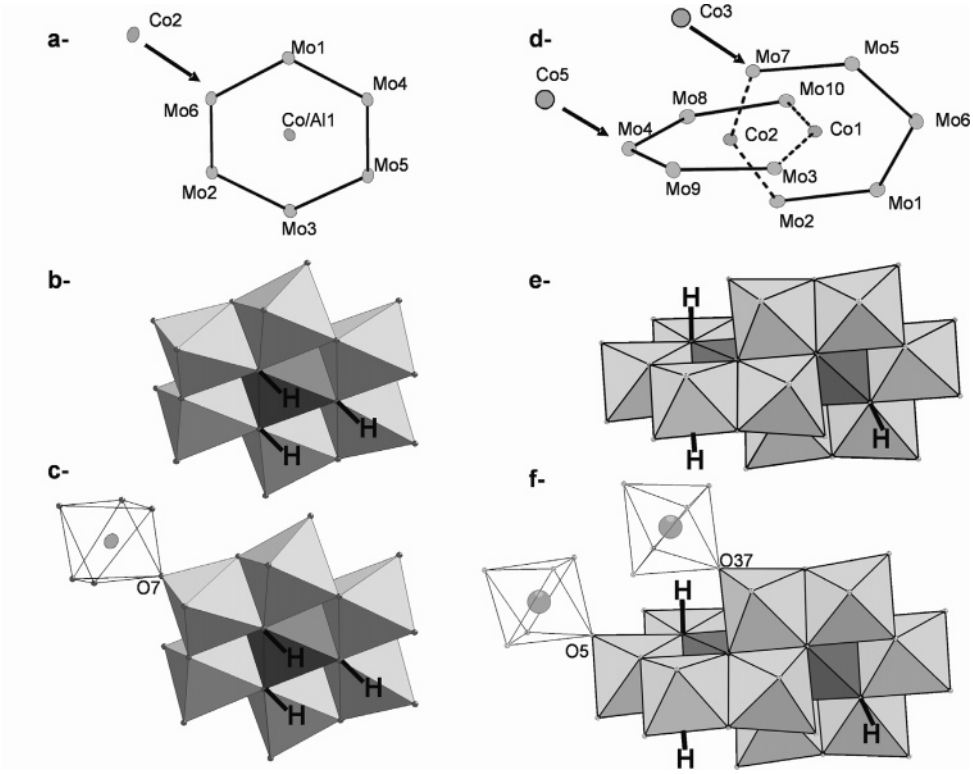

Figure 1. Mechanism of formation of the dimeric Co_2Mo_{10} HPA from the Anderson molybdocobaltate HPA. a. The Anderson HPA cationic framework with the extra Co(II) location. b. The resulting polyhedra linkage. c. The resulting cobalt salt new HPA. d−f. Same features for the Co_2MO_{10} HPA.

$mL \cdot min^{-1}$) of a H_2S/H_2 (10:90) mixture. Then the temperature was cooled to 573 K, and thiophene, purified by vacuum distillation, was introduced in the reactor at constant pressure (50 Torr) in a flow of hydrogen (20 $mL \cdot min^{-1}$). The reaction products (butane, butenes, etc.) were analyzed by a flame ionization detector gas chromatograph equipped with a plot-fused alumina column (stationary phase cp-Al_2O_3/KCl), and the conversion C was deduced according to the following formula:

$$C = \frac{\sum_i A_i/4}{A_{thio}/3.4 + \sum_i A_i/4}$$

where A_{thio} and A_i are the peak areas of respectively thiophene and the reaction products.

Results and Discussion

Elemental Analysis. Elemental analysis results for the ammonium and cobalt salts are in agreement with the expected formula as follows. $(NH_4)_6[Co_2Mo_{10}O_{38}H_4] \cdot 7H_2O$, elemental analysis (wt %) calculated (experimental): Co, 6.5 (5.7); Mo, 53.4 (49.5); N, 4.7 (4.3). $Co_3Co_2Mo_{10}O_{38}H_4$, elemental analysis (wt %) calculated (experimental): Co, 12.7 (12.1); Mo, 41.45 (40.2); N, 0 (<1). The Co/Mo and N/Mo ratios are reported in Table 1, in which the nomenclature used hereafter is also reported. For the two salts, the Co/Mo ratios obtained from chemical analysis are in agreement with the chemical formulas. The Co and Mo wt % values obtained by chemical analysis are almost equal to those expected from our calculation, the slight discrepancies being probably due to the minor presence of impurities. For the cobalt salt, the N/Mo ratio suggests a complete exchange of the ammonium by the Co atoms as revealed by the IR study. Indeed, the IR spectrum of $Co_2Mo_{10}Am$ (Supporting Information) exhibits the band at 1400 cm^{-1} characteristic of the NH_4^+ ions, and this band has completely disappeared upon exchange.

XRD Analysis. *$Co_2Mo_{10}Am$*. Evans and Showell[12] reported the preparation of two forms of the decamolybdodicobaltate-(III) ammonium salt named A and B and the crystal structure determination of B (monoclinic, $a = 12.59(1)$ Å, $b = 12.72(3)$ Å, $c = 15.48(1)$ Å, $\beta = 121.70(1)°$, space group *Pc*, $Z = 2$) leading to the $[Co_2Mo_{10}H_4O_{38}]^{6-} \cdot (NH_4)_6 \cdot H_2O$ exact formula. Unfortunately, crystallographic data are not available in their article nor in the JCSD. Cabello et al.[15] recently prepared the A form and simulated its X-ray powder pattern using the parameter given by Evans ($a = 44.18(3)$ Å, $b = 12.60(1)$ Å, $c = 15.36(1)$ Å, $\beta = 106.89(2)°$, space group *Cc* or *C*2/*c*). Our study concerned the B form, and the crystal structure determination has been performed in the *Pn* symmetry group with a reoriented unit cell. The $(NH_4)_6[H_4Co_2Mo_{10}O_{38}] \cdot 7H_2O$ formula is confirmed with, however, some ambiguity between water molecule and ammonium group assignments. The final reliability factors are R1 = 4.44, wR2 = 11.61. The crystal data are available as Supporting Information.

$Co_2Mo_{10}Co$. The crystal structure was satisfactorily refined in the *Cc* space group. The deduced formula is $Co_2Mo_{10}H_4O_{38}[Co(H_2O)_5]_2 \cdot (Co(H_2O)_6)_1 \cdot (H_2O)_9$, which implies no ambiguity regarding the interstitial H_2O molecule, considering Co(III) for the HPA central cobalt and Co(II) for additional cobalt.

As suggested by Evans and Showell, the dimeric $[H_4Co_2Mo_{10}O_{38}]^{6-}$ HPA can be deduced from the Anderson $H_6CoMo_6O_{24}$ group by removing one MoO_{2t} (where t stands

Table 3. Selected Distances (Å) for $[Co_2Mo_{10}O_{38}H_4]^{6-}(Co^{2+})_3(H_2O)_9$ and $[Co_2Mo_{10}O_{38}H_4]^{6-}(NH_4^+)_6(H_2O)_7$

	Co_2Mo_{10}(Co)		Co_2Mo_{10}(am)			Co_2Mo_{10}(Co)		Co_2Mo_{10}(am)	
Mo1−O27	1.709(3)	1.71	1.715(7)	1.68	Mo6−O38	1.706(7)	1.72	1.687(7)	1.81
Mo1−O12	1.715(7)	1.68	1.711(7)	1.70	Mo6−O24	1.710(7)	1.70	1.704(7)	1.73
Mo1−O35	1.943(6)	0.91	1.925(7)	0.95	Mo6−O35	1.929(6)	0.94	1.926(6)	0.95
Mo1−O34	1.947(6)	0.90	1.954(6)	0.86	Mo6−O26	1.938(6)	0.92	1.962(7)	0.86
Mo1−OH33	2.270(6)	0.38	2.266(5)	0.38	Mo6−OH8	2.255(5)	0.39	2.268(6)	0.38
Mo1−O31	2.346(6)	0.31	2.295(5)	0.35	Mo6−OH33	2.297(6)	0.35	2.279(6)	0.37
	$\sum S_{ij} = 5.87$		$\sum S_{ij} = 5.92$			$\sum S_{ij} = 6.03$		$\sum S_{ij} = 6.10$	
Mo2−O3	1.711(7)	1.70	1.698(7)	1.76	Mo7−O9	1.684(6)	1.83	1.691(6)	1.70
Mo2−O19	1.713(6)	1.69	1.740(6)	1.57	Mo7−O37	1.719(6)	1.66	1.709(6)	1.79
Mo2−O34	1.884(6)	1.06	1.901(6)	1.02	Mo7−O15	1.866(6)	1.12	1.895(6)	1.79
Mo2−O22	2.008(5)	0.76	1.989(6)	0.80	Mo7−O28	1.989(5)	0.80	1.998(5)	0.78
Mo2−O31	2.288(5)	0.36	2.273(6)	0.37	Mo7−O7	2.231(5)	0.42	2.277(6)	0.37
Mo2−O6	2.335(6)	0.31	2.287(5)	0.36	Mo7−O21	2.291(6)	0.35	2.339(5)	0.31
	$\sum S_{ij} = 5.88$		$\sum S_{ij} = 5.88$			$\sum S_{ij} = 6.18$		$\sum S_{ij} = 5.99$	
Mo3−O20	1.662(7)	1.94	1.686(5)	1.82	Mo8−O30	1.680(6)	1.85	1.705(7)	1.73
Mo3−O18	1.730(6)	1.61	1.726(6)	1.63	Mo8−O13	1.716(7)	1.68	1.710(7)	1.70
Mo3−O10	1.900(6)	1.02	1.889(5)	1.05	Mo8−O25	1.938(6)	0.92	1.926(6)	0.94
Mo3−O7	2.003(5)	0.77	2.016(6)	0.74	Mo8−O14	1.968(6)	0.85	1.937(6)	0.92
Mo3−O28	2.275(5)	0.37	2.279(5)	0.37	Mo8−OH17	2.236(6)	0.41	2.265(5)	0.39
Mo3−O6	2.321(6)	0.32	2.296(6)	0.35	Mo8−O22	2.314(5)	0.33	2.323(6)	0.32
	$\sum S_{ij} = 6.03$		$\sum S_{ij} = 5.96$			$\sum S_{ij} = 6.03$		$\sum S_{ij} = 6.00$	
Mo4−O23	1.704(7)	1.73	1.701(7)	1.70	Mo9−O29	1.691(7)	1.79	1.692(6)	1.79
Mo4−O5	1.743(7)	1.56	1.722(7)	1.68	Mo9−O16	1.695(7)	1.77	1.708(6)	1.71
Mo4−O14	1.911(6)	0.99	1.931(6)	0.95	Mo9−O36	1.950(6)	0.89	1.900(6)	1.02
Mo4−O36	1.962(6)	0.86	1.962(6)	0.88	Mo9−O10	1.963(6)	0.86	2.004(6)	0.77
Mo4−OH11	2.245(6)	0.40	2.263(6)	0.38	Mo9−OH11	2.257(6)	0.39	2.287(5)	0.36
Mo4−OH17	2.260(6)	0.39	2.265(5)	0.35	Mo9−O28	2.305(5)	0.34	2.297(5)	0.35
	$\sum S_{ij} = 5.93$		$\sum S_{ij} = 5.94$			$\sum S_{ij} = 6.05$		$\sum S_{ij} = 6.00$	
Mo5−O32	1.685(7)	1.82	1.685(7)	1.82	Mo10−O4	1.693(6)	1.78	1.692(6)	1.75
Mo5−O2	1.695(7)	1.77	1.702(6)	1.74	Mo10-O1	1.719(7)	1.66	1.708(7)	1.65
Mo5−O26	1.913(6)	0.98	1.927(6)	0.95	Mo10−O25	1.906(6)	1.00	1.899(6)	0.94
Mo5−O15	1.963(6)	0.86	1.943(6)	0.91	Mo10−O31	2.002(5)	0.77	2.004(5)	0.86
Mo5−OH8	2.272(6)	0.37	2.269(6)	0.38	Mo10−O22	2.261(5)	0.38	2.287(5)	0.38
Mo5−O7	2.361(5)	0.29	2.311(5)	0.34	Mo10−O21	2.308(6)	0.34	2.297(5)	0.38
	$\sum S_{ij} = 6.11$		$\sum S_{ij} = 6.13$			$\sum S_{ij} = 5.94$		$\sum S_{ij} = 5.95$	
Co1−O6	1.871(6)	0.63	1.881(6)	0.61	Co3−OH2h	2.058(6)	0.37		
Co1−O21	1.871(6)	0.63	1.869(6)	0.63	Co3−OH2i	2.066(7)	0.36		
Co1−O31	1.875(6)	0.62	1.889(5)	0.60	Co3−OH2f	2.067(6)	0.36		
Co1−O7	1.904(6)	0.58	1.899(5)	0.58	Co3−O37	2.076(6)	0.35		
Co1−OH33	1.930(6)	0.54	1.924(5)	0.55	Co3−OH2g	2.083(5)	0.35		
Co1−OH8	1.950(5)	0.51	1.947(6)	0.51	Co3−OH2j	2.156(6)	0.29		
	$\sum S_{ij} = 3.51$		$\sum S_{ij} = 3.49$			$\sum S_{ij} = 2.09$			
Co2−O21	1.860(6)	0.65	1.870(6)	0.63	Co4−OH2k	2.057(6)	0.37		
Co2−O6	1.874(6)	0.63	1.864(6)	0.64	Co4−OH2p	2.066(6)	0.36		
Co2−O28	1.904(5)	0.58	1.901(5)	0.58	Co4−OH2l	2.097(6)	0.33		
Co2−O22	1.908(5)	0.57	1.887(5)	0.60	Co4−OH2n	2.100(4)	0.33		
Co2−OH11	1.954(6)	0.50	1.948(5)	0.51	Co4−OH2m	2.113(4)	0.32		
Co2−OH17	1.958(6)	0.50	1.955(6)	0.50	Co4−OH2o	2.156(3)	0.29		
	$\sum S_{ij} = 3.42$		$\sum S_{ij} = 3.47$			$\sum S_{ij} = 2.01$			
Co1−Mo10	3.014(1)		3.010(2)		Co5−OH2d	2.042(4)	0.39		
Co1−Mo3	3.023(1)		3.031(2)		Co5−O5	2.064(4)	0.37		
Co1−Mo7	3.220(2)		3.256(2)		Co5−OH2c	2.065(5)	0.36		
Co1−Mo5	3.288(2)		3.261(3)		Co5−OH2a	2.090(6)	0.34		
Co1−Mo6	3.307(2)		3.302(2)		Co5−OH2b	2.097(6)	0.33		
Co1−Mo1	3.268(1)		3.263(1)		Co5−OH2e	2.17(1)	0.27		
Co1−Mo2	3.267(2)		3.240(3)			$\sum S_{ij} = 2.07$			
Co1−Mo8	5.243(3)		5.224(2)						
Co1−Mo4	6.074(4)		6.066(4)						
Co1−Mo9	5.228(3)		5.231(4)						
Co1−Co2	2.773(2)		2.771(2)						
Co3−Mo7	3.690(3)				Mo8−Mo2	4.171(2)		4.173(3)	
Co5−Mo4	3.764(3)				Mo8−Mo10	3.286(3)		3.249(3)	
					Mo8−Mo4	3.294(3)		3.304(3)	

for terminal oxygen atom) group from each of two Anderson HPAs, turning one ∼45° around the HPA equatorial plane and joining them so that the two CoO_6 octahedra share an edge. Figure 1 depicts this mechanism. In this figure, the additional exchanged cobalt positions with the label scheme for transition metals for both the previously described Anderson-type $Co/AlMo_6(Co)$[9] and $Co_2Mo_{10}(Co)$ are also shown. The resulting $[H_4Co_2Mo_{10}O_{38}]^{6-}$ block consists of a central Co_2O_{10} edge sharing dimer surrounded by two crowns of edge sharing MoO_6 octahedra, turned ∼45° from each other. Pertinent distances for both compounds are given in Table 3. In the cobalt salt, the additional cobalt cations Co3 and Co5 share the O37 and O5 corners, respectively, with the HPA. The free octahedral corners are constituted by OH_2 a−j molecules. The counter Co4 cation is isolated from the HPA and surrounded by six H_2O molecules (labeled OH_2 k−p). The interstitial water OH_2 molecules (1−9) are distributed around the block with distances to the peripheral HPA oxygen anions around 2.7 Å. The complete crystal structure is shown in Figure 2, highlighting the interstitial groups and the four equivalent HPAs generated by the *Cc* symmetry. It appears from Table 3 that intra-HPA Mo−O

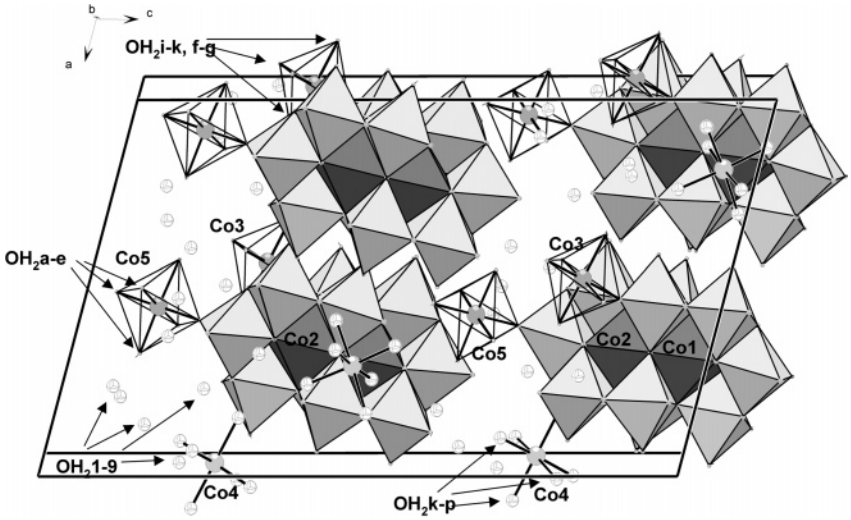

Figure 2. Crystal structure of the $[Co_2Mo_{10}H_4O_{38}(Co(H_2O)_5)_2]^{2-}\cdot[Co(H_2O)_6]_1\cdot(H_2O)_9$ compound.

distances remain nearly unchanged upon the NH_4^+ exchange by Co^{2+}. Even Mo4−O5 and Mo7−O37 are not drastically modified despite being corner-linked with the Co5 and Co3 counter-atoms, respectively.

Bond Valence Calculations. The valence bond sums, also reported in the Table 3, have been calculated using the Brese and O'Keefe data.[27] As for the Anderson HPA,[9] the Mo−O distances show three pairs of bonds, (i) short at ∼1.70 Å, (ii) medium at ∼1.95 Å, and (iii) long at ∼2.25 Å, unambiguously leading to valence bond sum calculations close to +6 [from Mo(VI) data, in Table 3]. It is well-known that the cobalt cations at the center of the $[H_4Co_2Mo_{10}O_{38}]^{6-}$ HPA are Co(III)[11] and are surrounded by oxygen atoms at Co−O distances included in the range 1.86−1.96 Å leading to $\sum S_{ij} \sim 3.5$, a value slightly higher than expected for trivalent cobalt. The additional Co3−5 coordination polyhedra are surrounded by oxygen/water molecules with longer Co−O, 2.04−2.17 Å assigned to Co(II), as confirmed by the bond valence calculations (see Table 3). For these latter species no significant bond length differences are observed between Co−O and Co−OH_2. Finally, one should remember that, as is already true for the Anderson salts, the dimeric $[H_4Co_2Mo_{10}O_{38}]^{6-}$ contains four characteristic hydroxide groups located on the central Co1−2 coordination polyhedra as in the $[H_6CoMo_6O_{24}]$ HPA.[9] Thus, for Co1, three types of oxygen are evidenced. O31 and O7 are linked to (Mo1, Mo2, Mo10, and Co1) and (Mo3, Mo7, Mo5, and Co1) leading to $\sum S_{ij} = -2.04$ and −2.03 for each one. O6 and O8 are linked to (Mo2, Mo3, Co1, and Co2) and (Mo7, Mo10, Co1, and Co2) respectively yielding $\sum S_{ij} = -1.87$ and −1.94. These values strongly suggest an O^{2-} nature for the four corners. On the opposite, OH8 and OH33 are only linked to the three cations (Mo5, Mo6, and Co1) and to (Mo1, Mo6, and Co1) leading to $\sum S_{ij} = -1.25$ and −1.26, respectively. The balance contribution to −2 strongly suggests the involvement of an OH bond. The same calculations performed for Co2 allow us to assign the hydroxide nature for OH11 and OH17. Then the H^+ protons likely complete $O(Mo_2Co_1H_1)$ tetrahedra with OH pointing perpendicularly to the crown plane.

The powder XRD patterns of $Co_2Mo_{10}Am$ and Co_2Mo_{10}-Co show the presence of single-phase samples. The refined lattice parameters reported below are in good agreement with single-crystal data. It confirms the homogeneity of the prepared samples and the sole presence of the B form of the ammonium salt. As mentioned above, the crystal structure has been performed in a reoriented unit cell as well as compared to the values proposed by Evans and Showell.[12]

$Co_2Mo_{10}Am$:	$a = 12.58(1)$ Å	$Co_2Mo_{10}Co$:	$a = 15.81(1)$ Å
	$b = 12.72(1)$ Å		$b = 13.11(1)$ Å
	$c = 13.93(1)$ Å		$c = 17.13(1)$ Å
	$\beta = 108.74(6)°$		$\beta = 105.91(5)°$

TGA-MS Analysis. TGA curves under pure helium of the ammonium and cobalt salts are shown in Figure 3. For $Co_2Mo_{10}Co$, three zones can be distinguished in the TGA curve, that is, zone A at temperatures below 100 °C, zone B for temperatures between 100 and 180 °C, and zone C corresponding to the final plateau after 400 °C. The MS analysis relative to H_2O ($m/e = 18$) is also presented in Figure 3. It allows us to clearly assign the first peak at 80 °C to the loss of hydration/coordination water, the second one centered at 170 °C to the loss of the coordination water around Co^{2+} countercations, and the last one spreading between 230 and 360 °C to the departure of the constitution water. This last step induces a destruction of the structure giving rise to the formation of the MoO_3 and $CoMoO_4$ oxides, as shown by XRD and Raman spectroscopy analysis (not reported here). An experimental total weight loss equal to 18.1% is observed, a value that is in agreement with the calculation (21%) based on the following equation:

$$Co_2Mo_{10}O_{38}H_4\cdot[Co(H_2O)_5]_2\cdot Co(H_2O)_6\cdot 9H_2O \rightarrow 5CoMoO_4 + 5MoO_3 + 18H_2O + {}^1/_2O_2$$

The major presence of $CoMoO_4$ clearly indicates the reduction of Co^{3+} into Co^{2+} ions, in the same way the MS curve ($m/e = 32$) relative to O_2 reveals the oxidation of H_2O into O_2. However, the aforementioned decomposition reaction into

(27) Brese, N. E.; O'Keefe, M. *Acta Crystallogr., Sect. B* **1991**, *47*, 192−197.

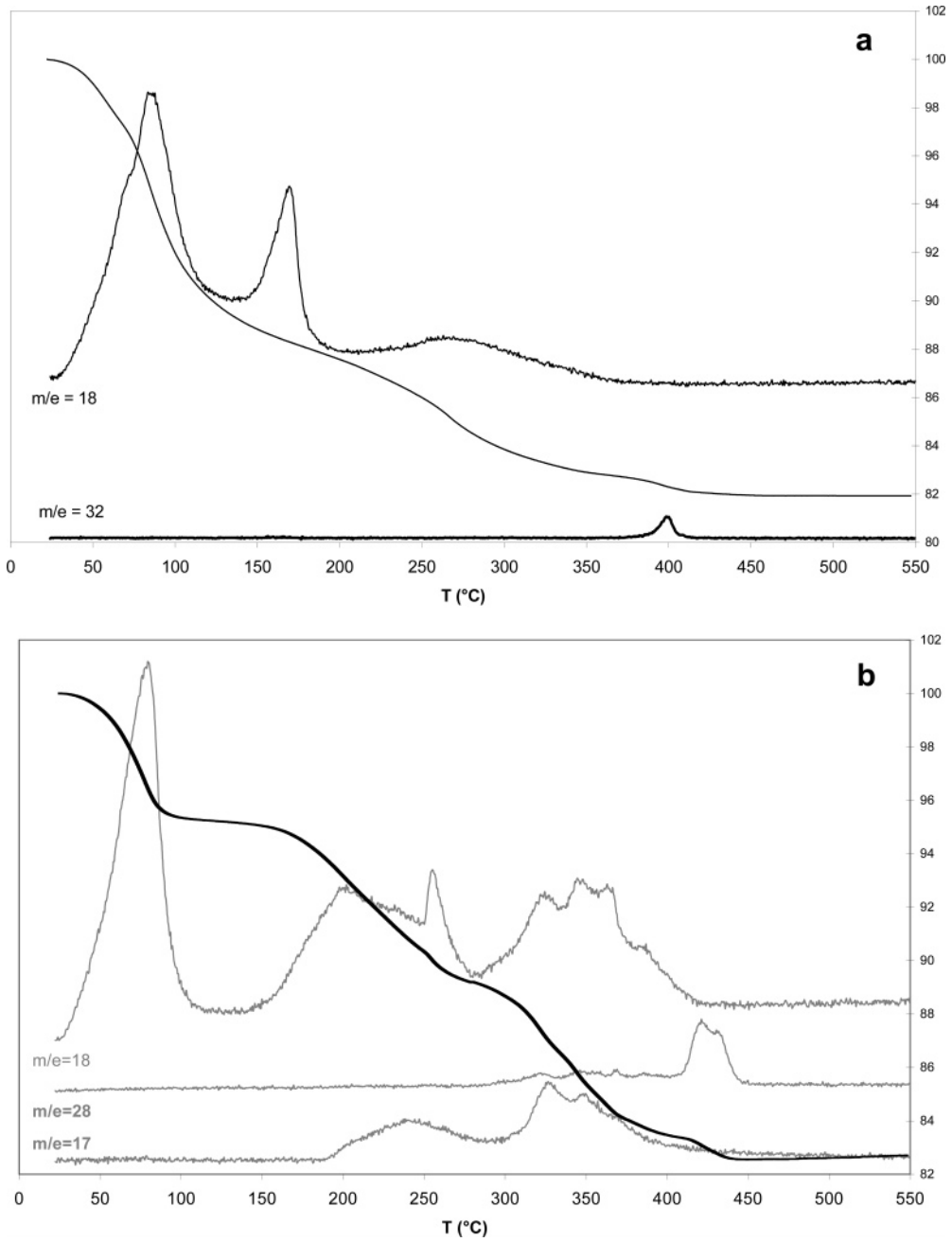

Figure 3. TGA (thick black line) and MS (thin grey lines) spectra under He of $Co_2Mo_{10}Co$ (a) and $Co_2Mo_{10}Am$ (b) solids.

$CoMoO_4$ could be not complete, and the persistence of some Co^{III} and/or oxy-hydroxy cobalt(II) may explain the small differences between the observed and the calculated weight losses.

For the ammonium salt, the experimental total weight loss (17.3%) is more important for $Co_2Mo_{10}Am$ and the plateau appears before 450 °C. The MS data can explain the $Co_2Mo_{10}Am$ TGA curve. The profile of the curve relative to H_2O ($m/e = 18$) indicates that the first peak corresponds to the loss of hydration water and is observed at 80 °C as for the cobalt salt. The two following peaks attributed to the loss of constitution water present several components spreading from 160 to 260 °C and from 280 to 400 °C. The MS analysis also shows peaks at *m*/*e* equal to 17 and 28 corresponding to NH_3 and N_2, respectively. The gas-phase NH_3 is coming directly from the decomposition of the ammonium groups that occurs from 200 to 400 °C, whereas the presence of N_2 after 400 °C can be explained by the oxidation of NH_3. This latter phenomenon is parallel to the cobalt reduction leading to the formation of $CoMoO_4$ as mentioned for the cobalt dimeric salt. Moreover a partial molybdenum reduction (Mo^{6+} into Mo^{5+}) is also evidenced by XRD analysis after calcination. Indeed, the XRD pattern evidenced the presence of Mo_4O_{11} with MoO_3 and $CoMoO_4$.

The following equation that may explain the transformation leads to a theorical total weight loss of 18% in agreement with the experimental value.

$$Co_2Mo_{10}O_{38}H_4(NH_4)_6{\cdot}7H_2O \rightarrow 2CoMoO_4 + 4MoO_3 + Mo_4O_{11} + 6NH_3 + 10H_2O + 2O_2$$

XAS. The EXAFS measurements would be helpful to characterize the preservation of the structure upon deposition on the alumina support for the preparation of the HDS oxidic

Table 4. Refinement of the EXAFS Signals of the Salts[a]

a. Refinement at the Mo K Edge

	Mo−O (1)	Mo−O (2)	Mo−O (3)	Mo−Mo	Mo−Co
			Co_2Mo_{10}(Am)		
N (exp)	1.99 (2)	2.01 (2)	2.11 (2)	1.98 (2)	0.40 (0.7)
R (Å) (exp)	1.69 (1.70)	1.93 (1.94)	2.29 (2.28)	3.31 (3.28)	3.21 (3.19)
$\Delta\sigma$ (Å)	0.04	0.09	0.06	0.08	0.09
ΔE (eV)			−2.22		
residue			0.01		
			Co_2Mo_{10}(Co)		
N (exp)	2.04 (2)	2.02 (2)	1.99 (2)	1.96 (2)	0.45 (0.7)
R (Å) (exp)	1.71 (1.70)	1.94 (1.94)	2.31 (2.29)	3.36 (3.29)	3.31 (3.20)
$\Delta\sigma$ (Å)	0.04	0.08	0.08	0.08	0.09
ΔE (eV)			1.29		
residue			0.008		

b: refinement at the Co K edge

	Co−O (1)	Co−O (2)	Co−Co	Co−Mo (1)	Co−Mo (2)
			Co_2Mo_{10}(Am)		
N (exp)	5.99 (6)		1.00 (1)	2.38 (2)	5.00 (5)
R (Å) (exp)	1.90 (1.90)		2.81 (2.77)	3.00 (3.02)	3.29 (3.26)
$\Delta\sigma$ (Å)	0.05		0.06	0.08	0.07
ΔE (eV)				0.12	
residue				0.036	
			Co_2Mo_{10}(Co)		
N (exp)	5.01 ($6 \times 2/5$)[b]	1.20 ($6 \times 3/5$)[b]	0.54 (2/5)	0.4 ($2 \times 2/5$)[c]	2.45 ($5 \times 2/5$)[c]
R (Å) (exp)	1.94 (1.90)	2.15 (2.09)	2.79 (2.77)	2.98 (3.02)	3.29 (3.27)
$\Delta\sigma$ (Å)	0.09	0.02	0.07	0.06	0.08
ΔE (eV)			−0.41		
residue			0.083		

[a] (exp): expected values for *R* and *N* from XRD single-crystal analysis. [b] Co^{2+} (3/5 of the total Co) and Co^{3+} (2/5 of Co) are both octahedrally coordinated with different mean Co−O bonds. [c] The Co^{2+}−Mo bonds being too long to be refined, Co^{3+} (2/5 of the total Co) is shortly bonded to two Mo ($d \sim 3$ Å) and five Mo with a greater separation ($d \sim 3.3$ Å).

precursor. EXAFS study of the starting bulk HPC has, therefore, been performed to obtain reference data for the EXAFS study of the alumina-supported sample but also to check the above XRD results.

EXAFS at the Mo K Edge. EXAFS oscillations were analyzed to obtain detailed structural information. For all the simulations, the crystallographic data deduced from the XRD study, numbers of neighbors and distances, have been used to create amplitude and phase functions with the FEFF program to fit the experimental EXAFS oscillations with the software "Round Midnight". The Mo K-edge spectra and the Fourier transform modulus of the $Co_2Mo_{10}Am$ and $Co_2Mo_{10}Co$ samples are reported respectively in parts a and b of Figure 4. In both cases, the refinement was successful, as shown in Table 4a, which reports the main parameters of the refinement process, that is, the number of neighbors *N*, the distance *R* (Mo-X), the Debye−Waller factor $\Delta\sigma$, the shift in energy ΔE, and the residual residue. The spectrum of the cobalt salts appears very similar to the ammonium salt one, confirming that the HPA structure is maintained upon the ionic exchange of the counterions and confirming that the Mo−Co^{2+} distances (cobalt as counterions) are too large (around 3.76 Å) to have a significant contribution in the examined EXAFS oscillations (Figure 4). The first shell in the Fourier tranform spectra contains three contributions due to the three Mo−O distances (1.71, 1.94, and 2.31 Å) in complete agreement with values obtained from XRD single-crystal analysis, whereas the second shell contains the contributions of the Mo and Co^{3+} neighboring atoms of the HPA structure. As is typical for EXAFS experimental results, distances are obtained with a good accuracy, whereas concerning the number of neighbors, discrepancies can be noted, as observed for the number of Co in the second shell. Nevertheless, the results of the refinement are quite similar for both salts, only a small difference of 0.1 Å is evidenced on the second shell Mo−Co distance. Even if small variation can be observed between these two salts it is clear that

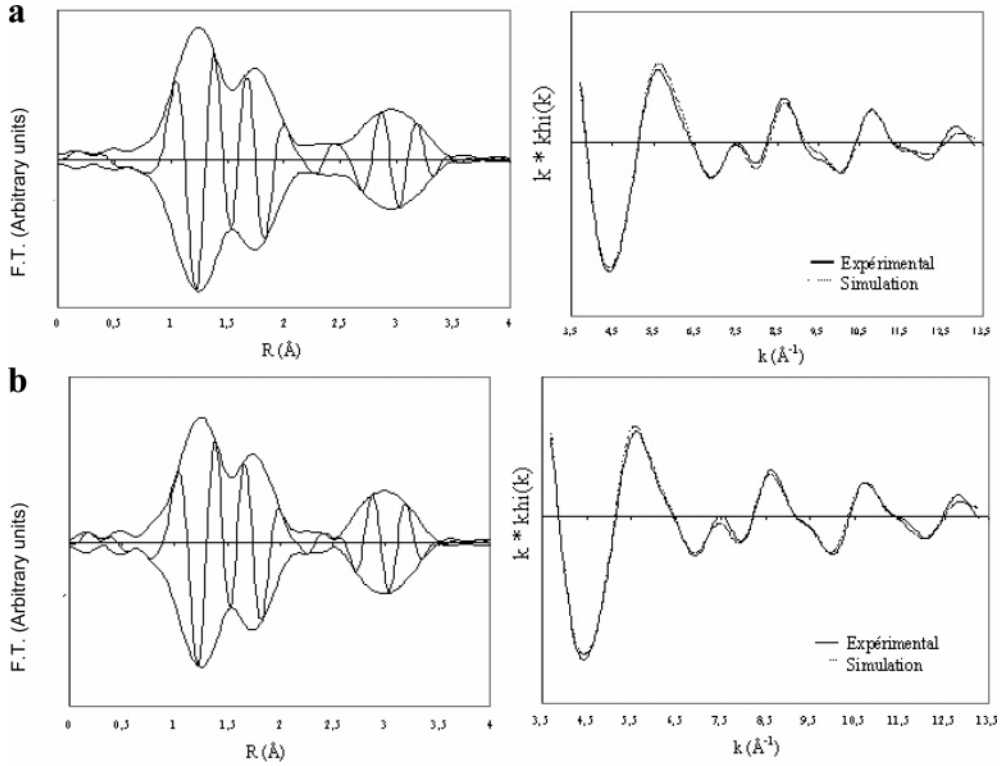

Figure 4. EXAFS at the Mo K edge of $Co_2Mo_{10}Am$ (a) and $Co_2Mo_{10}Co$ (b): (left) Fourier transform (3.7−13.4 $Å^{-1}$); (right) filtered EXAFS signal (0.83−3.47 Å) and signal simulated from FEFF contributions.

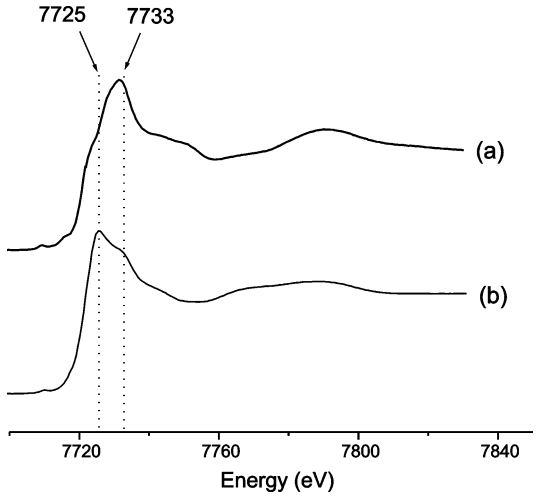

Figure 5. XANES spectra at the Co K edge of $Co_2Mo_{10}Am$ (a) and $Co_2Mo_{10}Co$ (b).

EXAFS results at the Mo K edge do not allow us to make the distinction between the ammonium and the cobalt salt of $Co_2Mo_{10}O_{38}H_4^{6-}$. EXAFS experiments at the Co K edge have, therefore, been performed.

XAS at the Co K Edge. (a) XANES. The position and shape of the Co K absorption edge mainly provide information about the oxidation state of the Co species. It is easy to distinguish between Co^{2+} and Co^{3+} ions, according to the shorter $Co^{III}-O$ distance determined by structural analysis, compared to the $Co^{II}-O$ distance. Indeed, the nonbonded and antibonded level of the Co^{3+} are less stabilized whereas the 1s level is more stabilized, leading to a higher transition energy. So, in Figure 5, the maximum peak present at 7733 eV for $Co_2Mo_{10}Am$ is assigned to Co^{3+}. As expected, the $Co_2Mo_{10}Co$ spectrum exhibits two peaks at 7725 and 7733 eV corresponding to Co^{2+} and Co^{3+}, respectively.

(b) EXAFS. In Figure 6 are reported the Co K-edge spectra and the Fourier transform modulus of the $Co_2Mo_{10}Am$ and $Co_2Mo_{10}Co$ samples. For the two samples, the refinement of the Co K-edge spectra was successful as indicated by the simulation. A simple examination of the figures indicates unambiguously that at the Co K edge the two samples can be distinguished. Each compound presents two shells. For the ammonium salt, the first shell corresponds to the sole $Co^{III}-O$ contribution with a cobalt oxygen distance of 1.90 Å and six neighboring oxygen atoms. In the second shell three types of contribution are evidenced, corresponding to the Co−Co contribution and to the two Co−Mo contributions according to the structural data. Each Co atom is surrounded in the second coordination shell by two Mo at 3 Å and five Mo at 3.29 Å, in agreement with XRD single-crystal analysis.

For $Co_2Mo_{10}Co$, the first shell is constituted of two contributions, $Co^{III}-O$ and $Co^{II}-O$. However, the $Co^{III}-O$ contribution appears overestimated ($N = 5$), because it was expected that two-fifths of the Co atoms were Co^{III}, the other ones being the Co^{II} countercations. Nevertheless, the two Co−O contributions with distances at 1.94 and 2.15 Å corresponding respectively to the $Co^{III}-O$ and the $Co^{II}-O$ groups are in good agreement with the structural data. This observation again confirms that EXAFS is reliable concerning the values of the distances obtained by the refinement whereas the number of neighbors is given with less accuracy. Nevertheless, the average total number of Co^{III} and Co^{II} oxygen neighbors, 6.21 (5.01 + 1.20), is close to the expected value of 6. In the second shell the same three contributions as for the ammonium salt are evidenced. They concern only the cobalt(III), the second neighbors of the Co^{II} being at too long a distance to be considered. The simulation results are in good agreement with the structural data that indicate that two-fifths of the cobalt atom owns one Co neighbor at 2.77 Å, two Mo at 3.02 Å, and five Mo at 3.27 Å. EXAFS at the Co K edge confirms the structural analysis of the ammonium and cobalt salts, and it indicates that this technique is a very precise tool for the characterization of these solids to clearly make the distinction between the ammonium and the cobalt salt.

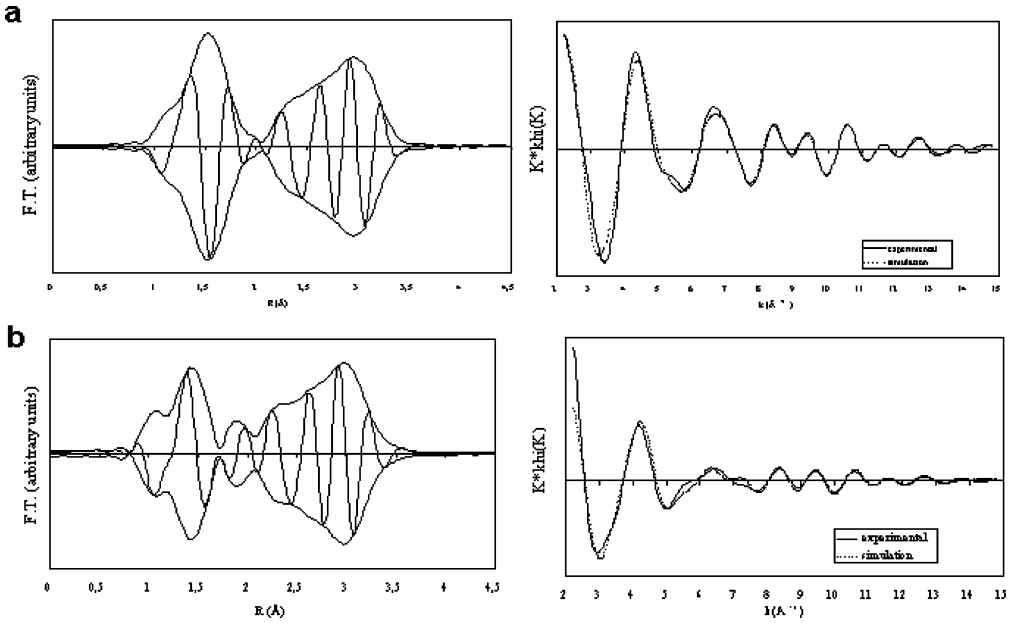

Figure 6. EXAFS at the Co K edge of $Co_2Mo_{10}Am$ (a) and $Co_2Mo_{10}Co$ (b): (left) Fourier transform (2.27−14.95 $Å^{-1}$); (right) filtered EXAFS signal (0.90−3.43 Å) and signal simulated from FEFF contributions.

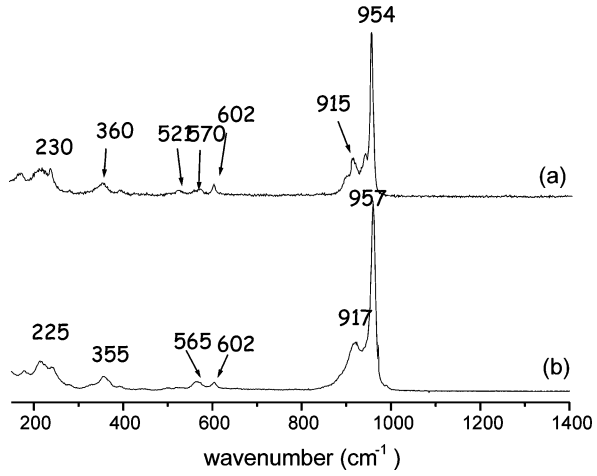

Figure 7. Raman spectra of bulk $Co_2Mo_{10}Am$ (a) and $Co_2Mo_{10}Co$ (b) solids.

Table 5. Assignment of the Vibrations of IR and Raman Spectra of $Co_2Mo_{10}Am$ and $Co_2Mo_{10}Co$[a]

$Co_2Mo_{10}Am$		$Co_2Mo_{10}Co$		
IR (cm^{-1})	Raman (cm^{-1})	IR (cm^{-1})	Raman (cm^{-1})	assignment
944 (vs)	954 (vs)	940 (vs)	957 (vs)	ν_{sym} Mo−O_{2t} (stretching)
855 (sh)	915 (sh)	908 (sh)	917 (sh)	ν_{as} Mo−O_{2t} (stretching)
679, 525 (m)	570, 521 (m)	690, 520 (m)	565 (m)	ν Mo−O−Co
486, 367, 322 (w)	360 (w)	480, 367, 320 (w)	355 (w)	δ Mo−O_{2t} (bending)

[a] vs, very strong; m, medium; w, weak; sh, shoulder.

Vibrational Spectroscopy. The Raman spectra are reported in Figure 7, whereas the IR ones are given in Supporting Information. The IR spectrum of $Co_2Mo_{10}Co$ is similar to the $Co_2Mo_{10}Am$ one, except for the absence of the N−H vibration band at 1400 cm^{-1}, which confirms the total exchange of the ammonium cations in the $Co_2Mo_{10}Co$ sample. The IR spectrum of the ammonium salt is in agreement with the one reported by Cabello.[15] On the basis of previous studies dealing with the Anderson compounds ($AlMo_6$ and $CoMo_6$ salts), an assignment of the main vibrational modes of the dimeric HPA is given in Table 5. The similarity of the IR, on one hand, and Raman features, on the other hand, of the cobalt and ammonium HPA salts gives also evidence for the preservation of the dimeric Anderson structure upon the cation exchange. However, if we cannot distinguish by Raman spectroscopy both types of salt, it is easy to discriminate the Anderson molybdocobaltate entity from the dimeric molybdocobaltate HPA. Indeed, a shift of the line characteristic of the MoO_{2t} stretching mode is observed (955 cm^{-1} for Co_2Mo_{10}, 949 cm^{-1} for $CoMo_6$).[28] Moreover, the shape and the position of the line characteristic of the Mo−O−Co vibrational mode significantly differ in these HPA structure.

DRS Spectra. Figure 8 shows the DRS spectra of $Co_2Mo_{10}Am$ and $Co_2Mo_{10}Co$. In this figure are also reported for comparison purposes the DRS spectra of the $Co(NO_3)_2 \cdot 6H_2O$ and of the $CoMo_6Am$, in which the Co are in octahedral configuration but with a 2+ and a 3+ oxidation state, respectively. Whatever the Mo-containing sample, a main band around 300 nm is observed that is assigned to the $O^{2-} \rightarrow Mo^{6+}$ charge transfer. The UV spectra of the

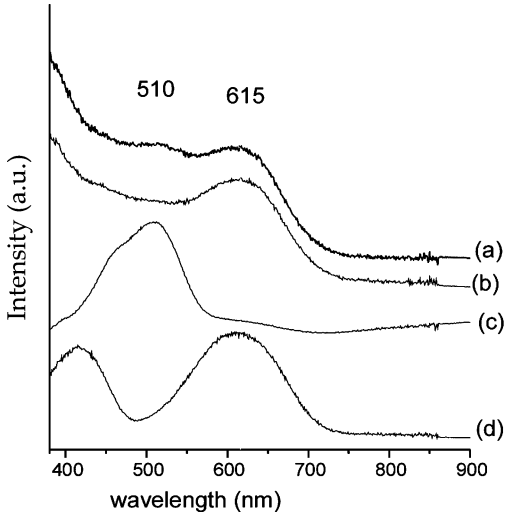

Figure 8. DRS spectra of bulk compounds. (a) $Co_2Mo_{10}Co$; (b) $Co_2Mo_{10}Am$; (c) $Co(NO_3)_2$; (d) $CoMo_6Am$.

reference samples clearly indicate that we can distinguish high-spin Co^{2+} atoms (d^7 configuration) from the low-spin Co^{3+} in octahedral configuration. The former one exhibits an absorption band in the 500−526 nm range, centered in our case at 510 nm, which is characteristic of the $^4T_{1g}(F) \rightarrow {}^4T_{1g}(P)$ transition. The $CoMo_6Am$ UV spectrum exhibits bands around 615 and 420 nm, which can respectively be assigned, according to literature data, to the $^1A_{1g} \rightarrow {}^1T_{1g}$ band and to the $^1A_{1g} \rightarrow {}^1T_{2g}$ transition of Co^{3+} low-spin atoms.[29,30] Thus, only Co^{3+} ions are evidenced in the $Co_2Mo_{10}Am$ with the band at 615 nm, the 420-nm band appearing as a shoulder on the aforementioned broad charge-transfer band. In the cobalt salt, these features are also observed with the band at 510 nm characteristic of the Co^{2+} ions. These results are, thus, in good agreement with the XANES data.

Catalytic Results. Thiophene HDS conversion of $Co_2Mo_{10}Co$-based catalysts versus molybdenum loading expressed as molybdenum weight % is presented in Figure 9, in which is also reported the conversion of reference catalysts (prepared with AHM and cobalt nitrate). For comparison purposes, the molecular Co/Mo ratio of the reference catalyst is maintained at 0.5, the value in $Co_2Mo_{10}Co$. The reference catalysts exhibit the classical "volcano" shaped curve[31] that is not observed for the HPA-based catalysts. Whatever the Mo loading, the $Co_2Mo_{10}Co$-based catalysts are more active than the reference ones. The improvement of the catalytic performances is due to a better efficiency of the cobalt-promoting effect as previously stated for Keggin-based catalysts.[6] This is assigned to the insertion of the Co within the $Co_2Mo_{10}Co$ precursot, avoiding cobalt loss inside the alumina support during the catalyst preparation. For both preparations a decrease of the conversion is observed at high Mo loading that is assigned to a loss of dispersion according

(28) Payen, E.; Plazenet, G.; Martin, C.; Lamonier, C.; Lynch, J.; Harle, V. *Stud. Surf. Sci. Catal.* **2002**, *143*, 141−148.
(29) Kosova, N. V.; Anufrienko, V. F.; Larina, T. V.; Rougier, A.; Aymard, L.; Tarascon, J. M. *J. Solid State Chem.* **2002**, *165*, 56−64.
(30) Cabello, C. I.; Botto, I. L.; Cabrerizo, F.; Gonzales, M. G.; Thomas, H. J. *Adhes. Sci. Technol.* **2000**, *18* (7), 591−608.
(31) Tøpsøe, H.; Clausen, B. S. *Appl. Catal.* **1986**, *25*, 273.

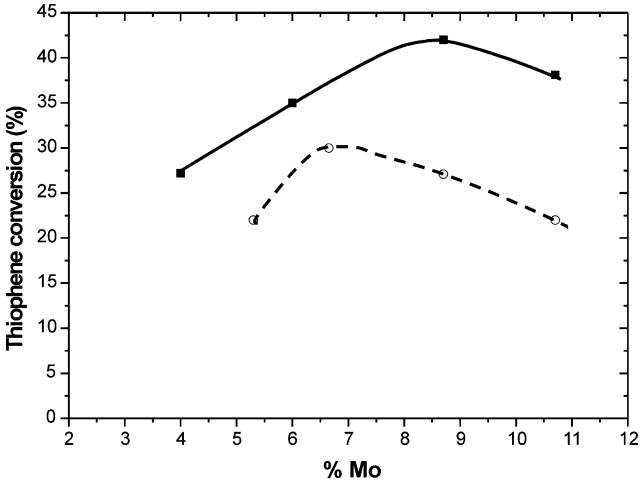

Figure 9. Catalytic performances expressed as thiophene conversion versus Mo loading (Mo wt %) for $Co_2Mo_{10}Co$-based catalysts (full line) and for conventional ones (dotted line).

to the literature data.[32] Nevertheless, the use of the HPA also allows improvement of the molybdenum dispersion at high Mo loading.

Conclusion

In this study, our attention has been particularly focused on derived Anderson-type HPA. The $Co_2Mo_{10}O_{38}H_4^{6-}$ cobalt salt has been prepared from the ammonium salt of the HPA by using ionic exchange in aqueous solution. The preparation method led to the complete exchange of the NH_4^+ ions as shown by IR spectroscopy and elemental analysis. IR and Raman spectroscopies clearly showed that the HPA structure is preserved upon the exchange, and the presence of Co in the two oxidation states has been clearly evidenced by UV spectroscopy as well as by XANES at the Co K edge. The X-ray structure resolution clearly showed that within the three Co^{2+} countercations only one $[Co(H_2O)_6]^{2+}$ is isolated from the dimeric structure, the two other $[Co(H_2O)_5]^{2+}$ entities being in fact directly linked through a bridged oxygen atom to each initial Anderson HPA structure (from which a MoO_{2t} group has been removed). This association creates the new dimeric structure. Thus, we evidenced the same principle of association of one Anderson structure and one linked $[Co(H_2O)_5]^{2+}$ as it has been shown for the cobalt salt of the six molybdocobaltate HPA^{4-}.[9] All these results were confirmed by XAS studies. Additional characterizations give us a database for the characterization of the solid after deposition on an alumina support for the preparation of HDS oxidic precursors. Moreover, preliminary HDS catalytic tests clearly show that the decamolybdocobaltate cobalt salt is an efficient precursor for the preparation of HDS catalysts, exhibiting a better promoting effect and a better dispersion of the molybdenum entities.

Supporting Information Available: Infrared spectra and powder diffraction patterns (TIF) and X-ray crystallographic files in CIF format. This material is available free of charge via the Internet at http://pubs.acs.org.

CM0503634

(32) Dufresne, P.; Payen, E.; Grimblot, J.; Bonelle, J. P. *J. Phys. Chem.* **1981**, *85*, 2344.